SOLAR POLARIZATION 5
ASP Conference Series, Vol. 405, © 2009
S. V. Berdyugina, K. N. Nagendra, and R. Ramelli, eds.

Full Magnetic Field Vector of an Emerging Flux Region

Z. Xu, A. Lagg, and S. K. Solanki

Max-Planck Institute for Solar System Research, Katlenburg-Lindau, Germany

Abstract. We present maps of the full magnetic field vector of an emerging flux region in both the photosphere and chromosphere. The magnetic and velocity structure of freshly emerged loops is determined.

1. Introduction

Solar magnetic fields are generated near the base of the solar convection zone through a dynamo mechanism, and rise to the solar surface due to buoyancy. The emerging field normally appears at the surface in the form of bipolar emerging flux regions (EFRs). The magnetic field vector of EFRs has been well studied in the photosphere (Brants 1985; Lites, Skumanich, & Martínez Pillet 1998; Bernasconi et al. 2002; Kubo, Shimizu, & Lites 2003; Centeno et al. 2007). At chromospheric heights, however the direct measurement of EFR vector magnetic fields was made only by Solanki et al. (2003) and Lagg et al. (2004, 2007) based on the Stokes I, Q, U and V profiles of He I 10830Å triplet. The He I triplet is a unique diagnostic tool for upper chromosphere magnetism owing to its optical thinness. Based on the magnetic field vector of each point in this region, Solanki et al. (2003) traced out chromospheric loops in 3 dimensions. So far, similar observations are rare and NOAA 9451 observed in 2001 is the only EFR studied. There is clearly a need to observe further similar regions, especially with an improved polarimeter. In this paper, we present observations made in 2006 of a young emerging flux region observed with the new Tenerife Infrared Polarimeter (TIP II) at the Vacuum Tower Telescope (VTT).

2. Observation

NOAA 10917 first appeared on 2006 October 20. It grew considerably in the following 24 hours and several bipolar pairs of pores began to emerge on October 21. We carried out spectropolarimetric observations with the TIP II polarimeter at the VTT in Tenerife on October 21. The active region was located at 05°S 34°W, with $\mu = \cos\theta = 0.81$. Full Stokes parameters I, Q, U and V were recorded with a spectral resolution of 30 mÅ. The 8 Å wide spectral window completely covers the photospheric line of Si I (10827.1Å) and the chromospheric He I 10830Å triplet.

The main difference from the previous observation of Solanki et al. (2003) are: (1) the Tenerife Infrared Polarimeter II (TIP II, Collados et al. 2007) was used to get a bigger field of view with higher spatial and spectral resolution

than TIP (Martínez Pillet et al. 1999); (2) We scanned this region with the slit parallel to the dark loop-like structures monitored by the Hα slit-jaw images, enabling us to observe an entire loop at the same time.

3. Model Atmosphere and Inversion Technique

The Stokes I, Q, U and V profiles of both the photospheric Si I line and the chromospheric He I line were fit using HeLIx code (Lagg et al. 2004), which is based on the analytic Unno-Rachkovsky solution to the radiative transfer equations of Zeeman-split lines in a Milne-Eddington model atmosphere. Eight parameters are used to fit the observed profiles: the strength of the magnetic field vector ($|B|$), its inclination (γ) and azimuth angle (χ), line-of-sight velocity (v_{LOS}), Doppler width ($\Delta\lambda_D$), damping constant (a), slope of the source function (S_1) and the opacity ratio between line-center and continuum (η_0). This code allows us to retrieve these parameters for multiple unresolved atmospheric components within a spatial resolution element. Another free parameter *filling factor* is needed to scale the different components relative to each other. For the Si I line we used a two-component atmospheric model composed of a magnetic and a field-free component. For the He I line, we assumed that the magnetic field fills the entire resolution element completely, but at some locations a multi-component model was still needed to account for multi-velocity components coexisting in one pixel (Lagg et al. 2007). In addition, we took into account the incomplete Paschen-Back effect (Sasso, Lagg, & Solanki 2006) and Hanle effect (Lagg et al. 2004) for He I triplet calculations.

4. Retrieved Map of the Magnetic Field Vector and LOS Velocity

Fig. 1 shows maps of the magnetic field vector and LOS velocity in the photosphere and chromosphere. In the photosphere they refer to the magnetic component, while in the chromosphere they are from the magnetic component with larger filling factor. The main observed properties of this EFR in these two layers are as follows :

- Photosphere: (1) There is no large scale and fast LOS velocity. The average speed is about 1 km/s. Downflows with velocity ~ 1.5 km/s are observed in some regions (marked by dotted squares in Fig. 1), close to the footpoints of loop-like structures seen in He I line center, where supersonic downflows are found in the upper chromosphere. (2) The magnetic field strength of the emergence zone is between 300 G and 600 G, and exceeds 1500 G when the field becomes more vertical in the sunspots. Note, however, that due to the use of a single line these values need not reflect the intrinsic field strength. (3) Bipolar features are present in the emerging zone, rather than in the moats of sunspots. The polarity of the part close to the sunspot is always opposite to that of sunspot itself. The two parts with opposite polarities stay connected during their lifetime (time series observations are not shown here) and there is no counterpart in the upper chromosphere.
- Chromosphere: (1) Dark elongated structures are found to connect two young opposite polarity sunspots (**a** and **b**). (2) Large scale LOS veloci-

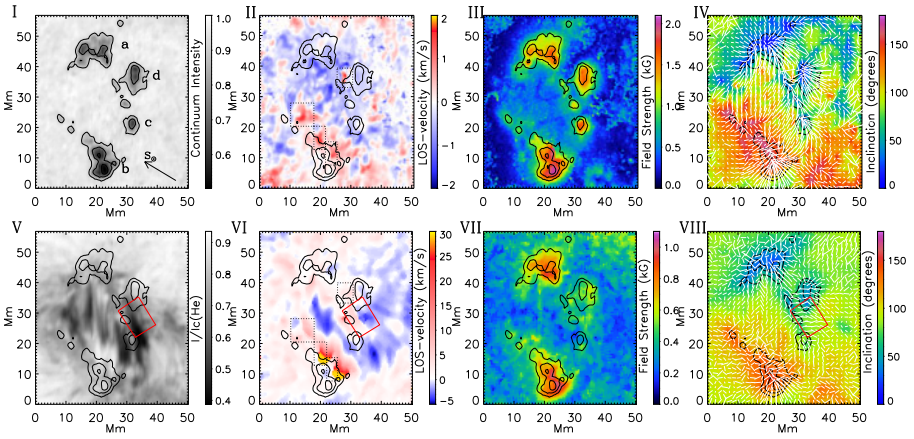

Figure 1. Atmospheric parameters of active region NOAA 10917 (October 21 2006, 16:28-16:51 UT) in the photosphere (top row) and in the chromosphere (bottom row). Panel I shows continuum intensity with the direction of solar disk-center marked by an arrow and sunspots **a-d** identified. Panel V displays the intensity ratio between the He I line core and the continuum to emphasize the absorption in dark loops. Panel II and VI are the line-of-sight velocity, III and VII, the magnetic field strength and IV and VIII the filed inclination angle with azimuth angle superposed (white lines). The contour lines in each panel indicate the sunspots for reference. The arrow points to the disk center.

ties of the loops are clearly present : upflows at the loop top and downflows along the loops' legs, supersonic downflows (> 10 km/s) are found at both ends of the loops. (3) The magnetic field strength in the emergence zone is below 300 G. (4) Field lines were traced based on the vector field information in each pixel. Using a series of constraints developed by Solanki et al. (2003), we identified the traced bundle of field lines with loops. We illustrate the loops in a 3-dimensional view in Fig. 2 and the typical variation of physical parameters along the magnetic field lines in Fig. 3. Note that in Fig. 2 the Z-axis scale is stretched and actually the loops are very shallow with an apex of 5 Mm, so that the magnetic field is principally horizontal. (4) A rotating filament is observed near the EFR with a vertical shear LOS velocity outlined by a red square in Fig. 1. The frozen magnetic field in the rotating mass flow can account for the orientation of the azimuth angles in this area.

Briefly, two young opposite polarity sunspots are connected by dark elongated striations in the upper chromosphere. The azimuth angle of both the photospheric and chromospheric field roughly follow these striations. The chromospheric field is more horizontal and homogeneous than the photosphere, particularly within the emergence zone. Bipolar magnetic features are only visible in photosphere rather than in the upper chromosphere. The magnetic field strength decreases from the photosphere to chromosphere. The maximum gradient of magnetic flux, 0.3 G km^{-1}, is found around sunspot **c**, above which the loops cross. The lowest flux gradient is about 0.1 G km^{-1} around one of the

loop footpoints, i.e. the following sunspot **b**. Based on the retrieved magnetic vector, we are able to reconstruct the magnetic field in 3 dimensions in upper chromosphere with constraints given by Solanki et al. (2003). Both the present and the previous results (Solanki et al. 2003) show asymmetric velocity and magnetic vector distribution along loops. However the present reconstructed loops are much shallower and more horizontal than the previous.

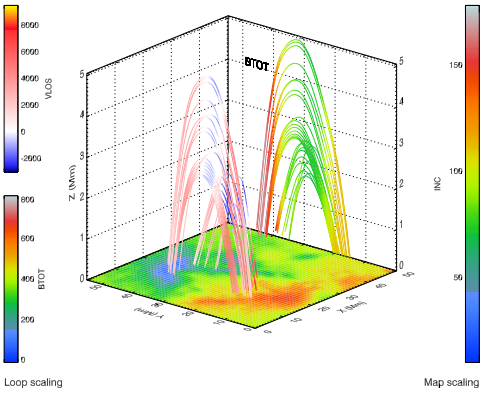

Figure 2. Three dimensional structure of chromospheric magnetic loops reconstructed from He I 10830Å Stokes inversion in an emerging flux region. The magnetic inclination map is plotted at the bottom and the loops are colored according to LOS velocity at each location. The magnetic field strength, represented by the colors of the loop, is projected on the Y-Z plane.

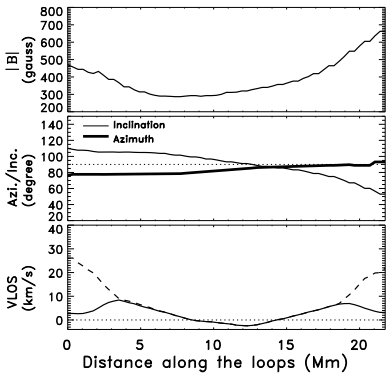

Figure 3. Variation of atmospheric parameters along a typical loop. The parameters from top to bottom are the magnetic field strength, field direction (azimuth and inclination are shown respectively as thick and thin solid lines) and LOS velocity. The dotted-line in the middle and bottom panels represent the 90° inclination angle (polarity reversal) and zero LOS velocity respectively. In the bottom panel, the dashed-line shows the co-existing LOS velocity component within one resolution pixel, which has a smaller filling factor than the one plotted as solid line.

References

Bernasconi, P. N., Rust, D. M., Georgoulis, M. K., & Labonte, B. J. 2002, Solar Phys., 209, 119

Brants, J. J. 1985, Solar Phys., 95, 15

Centeno, R., Socas-Navarro, H., Lite, B., Kubo, M., Frank, Z., Shine, R., Tarbell, T., Title, A., Ichimoto, K., Tsuneta, S., Katsukawa, Y., Suematsu, Y., Shimizu, T., & Nagata, S. 2007, ApJ, 666, L137

Collados, M., Lagg, A., Díaz Garcí A, J. J., Hernández Suárez, E., López López, R., Páez Mañá, E., & Solanki, S. K. 2007, in ASP Conf. Ser. Vol. 368, The Physics of Chromospheric Plasmas, ed. P. Heinzel, I. Dorotovič & R. J. Rutten (San Francisco: ASP), 611

Lagg, A., Woch, N., Krupp, N., & Solanki, S. K. 2004, A&A, 414, 1109

Lagg, A., Woch, J., Solanki, S. K., & Krupp, N. 2007, A&A, 462, 1147

Lites, B. W., Skumanich, A., & Martínez Pillet, V. 1998, A&A, 333, 1053

Kubo, M., Shimizu, T., & Lites, B. W. 2003, ApJ, 595, 465

Martínez Pillet, V., Collados, M., Sánchez Almeida, J., González, V., Cruz-Lopez, A., Manescau, A., Joven, E., Paez, E., Diaz, J., Feeney, O., Sánchez, V., Scharmer, G., & Soltau, D. 1999, in ASP Conf. Ser. Vol. 183, High Resolution Solar Physics: Theory, Observations, and Techniques, ed. T. R. Rimmele, K. S. Balasubramaniam & R. R. Radick (San Francisco: ASP), 264

Sasso, C., Lagg, A., & Solanki, S. K. 2006, A&A, 456, 367

Solanki, S. K., Lagg, A., Woch, J., Krupp, N., & Collados, M. 2003, Nat, 425, 692